



## Analysis of Resonance Transitions in X-Ray Spectra of Electron Interaction with Highly Charged Iron Ions

LI Yue-Ming<sup>1)†</sup>, KATO Daiji<sup>2)†</sup>, TONG Xiao-Min<sup>2)†</sup>, WATANABE Hirofumi<sup>2)†</sup>, WATANABE Tsutomu<sup>2)†</sup>, O'ROURKE Braian<sup>3)</sup>, KURAMOTO Hideharu<sup>2)†</sup>, NAKAMURA Nobuyuki<sup>2)†</sup>, CURRELL Frederick J.<sup>2,3)</sup>, YAMADA Chikashi<sup>1,2)</sup> and OHTANI Shunsuke<sup>1,2)</sup>

<sup>1)</sup> *Institute for Laser Science, The University of Electro-Communications, Chofu 182-8585, Japan*

<sup>2)</sup> *Cold Trapped Ions Project, ICORP, JST, Tokyo 182-0024, Japan*

<sup>3)</sup> *Department of Pure and Applied Physics, Queen's University, Belfast, BT7 1NN, U.K.*

(Received 27 September 2002 / Accepted 5 December 2002)

### Abstract

In electron interactions with highly charged Fe ions, the X-ray spectra were theoretically analysed and compared with the experimental results at the Tokyo EBIT. In the present analysis, cross sections for dielectronic recombination, resonance excitation, resonance recombination, and direct excitation were calculated by use of the distorted wave method. Simulated spectra were obtained by convoluting the calculated cross sections with the experimental beam energy resolution and X-ray detector resolution, which are in close agreement with the experimental observations. Based on our calculations including polarization effects, we estimate the charge state balance: He-like Fe<sup>24+</sup> (74%), Li-like Fe<sup>23+</sup> (18%), and Be-like Fe<sup>22+</sup> (8%), and the ion density in the trap to be  $6.5 - 8.5 \times 10^8 \text{ cm}^{-3}$ . The present calculations were also compared with the previous high-resolution measurements of the KLL resonances in He-like Fe ions.

### Keywords:

dielectronic recombination, highly charged iron ion, plasma spectroscopy, ebit

### 1. Introduction

In electron interactions with highly charged ions, electrons in a bound state of a highly charged ion form many-fold electronic open channels combined with an

incident electron. These open channels can interact strongly with closed channels of the discrete doubly excited states in the continuum, especially in the case that the energies of the open and closed channels are

---

author's e-mail: dkato@nifs.ac.jp

†Present Address

LI Yue-Ming, *Institute of Applied Physics and Computational Mathematics, Beijing 100088, P.R. China*

KATO Daiji, *National Institute for Fusion Science, Toki 509-5292, Japan*

TONG Xiao-Min, *Kansas State University, Manhattan, Kansas 66506, U.S.*

WATANABE Hirofumi, *Queen's University, Belfast, BT7 1NN, U.K.*

WATANABE Tsutomu, *Institute for Laser Science, The University of Electro-Communications, Chofu 182-8585, Japan*

KURAMOTO Hideharu, *Hitachi Engineering Co., Ltd., Ibaraki 319-1221, Japan*

NAKAMURA Nobuyuki, *RIKEN, Wako 351-0198, Japan*

nearly equal. As a result, this interaction would lead to a specific final state, which is called the resonance transition. The resonance processes may contribute remarkably to the cross sections [1]. The Electron Beam Ion Trap (EBIT) is an effective device for investigating such processes at high energy interaction regions, since this device uses a high energy mono-energetic electron beam to generate, trap, and probe highly charged ions [2,3].

Observations of electron-ion interactions for very highly charged Fe ions are especially important for applications to solar and TOKAMAK plasmas due to its high abundance. For He-like  $\text{Fe}^{24+}$  ions, the electron impact excitation cross sections have been measured using the EBIT at the Lawrence Livermore National Laboratory [4]. Beiersdorfer *et al.* [5] have also investigated dielectronic recombination resonances through  $1s2l2l'$  states by high-resolution X-ray spectroscopy.

Recently, at the Tokyo EBIT facility [6-8] X-ray spectra from highly charged Fe ions have been observed at electron beam energies ranging from 4.3 keV to 7.86 keV [9]. In this energy region, the dominant ionic species produced in the trap is considered to be He-like ions, while H-like ions cannot be produced since the ionization potential of He-like Fe ion (8.825 keV) is larger than the present maximum beam energy. In the present paper, theoretical calculations which may be compared with the experimental results have been performed for several contributions in the electron-ion interaction due to dielectronic recombination (DR), resonant excitation (RE), resonance recombination (RER) and direct excitation (DE). However, radiative recombination (RR) processes are not discussed in this paper since these contributions to the spectra are considered to be negligible for the present electron energies and densities in the interaction.

In the present analysis, cross sections of the processes concerned were calculated using the isolated resonance approximation. Auger decay rates and radiative decay rates were obtained by using the multi-configuration Hartree-Fock method with relativistic corrections [10,11]. The continuum states were described by distorted waves in the potential chosen to be the same as that for the bound states. The DE cross sections were calculated by using a fully relativistic distorted wave approximation method based on the GRASP code [12] similar to that described in the work of Zhang and Sampson [13].

## 2. Basic Theory

In the DR process, an incident free electron is captured in an excited state and one of the bound electrons in the target ion is simultaneously excited to another excited orbital to resonantly form a doubly-excited state. In the second step, this state decays to a singly excited state through photon emission. In the case of the target ions having more than two electrons, the DR process is represented schematically as

$$1s^2\beta + e \rightarrow 1s2l\beta nl' \rightarrow 1s^2\beta nl' + h\nu$$

for the inner  $2l$  electron decay and

$$1s^2\beta + e \rightarrow 1s2l\beta nl' \rightarrow 1s^22l\beta + h\nu'$$

for the outer  $nl'$  electron decay, where  $\beta$  is considered to be one or more spectator electrons in this process. For Li- and Be-like ions, the  $\beta$  corresponds to one or two electrons in the 2s shell, while in He-like ions there is no  $\beta$  electron.

The first step in the above expressions (the resonant electron capture) is the inverse of auto-ionization (Auger) process. Using an isolated resonance approximation to investigate the DR resonance processes, the electron capture cross section from the initial ionic target state  $a$  to the intermediate doubly-excited state  $i$  can be expressed by the product of the Auger decay rate and the Lorentzian-shaped profile function multiplied by the statistical weight factor. Since there are two possible decays from the intermediate  $i$  state, that is, radiative and Auger decays, the DR cross section to form the final singly-excited state  $k$  through photon emission must involve the fluorescence yield. Consequently, the DR cross section for  $a \rightarrow i \rightarrow k$  can be written in atomic units as

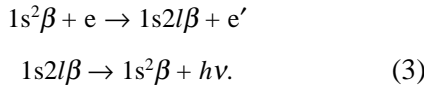
$$\sigma_{aik}^{\text{DR}}(E_e) = \frac{\pi^2}{E_e} \frac{g_i}{2g_a} A_{ia}^a \frac{\frac{\Gamma_i}{2\pi}}{(E_e - E_{ia})^2 + \frac{\Gamma_i^2}{4}} \frac{A_{ik}^r}{A_i^r + A_i^a}. \quad (1)$$

Here  $E_{ia}$  is the energy difference between  $i$  and  $a$ ,  $E_e$  the incident electron energy,  $A_{ia}^a$  the Auger decay rate from  $i$  to  $a$ ,  $A_{ik}^r$  the radiative decay rate from  $i$  to  $k$ , and  $A_i^r$  and  $A_i^a$  are the total Auger and radiative decay rates from  $i$ , respectively.  $g_i$  and  $g_a$  are the statistical weights of  $i$  and  $a$ , respectively.  $\Gamma_i = A_i^r + A_i^a$  is the width of the resonance. The middle term in Eq. (1) indicates the so-called Lorentzian-shaped profile function with width  $\Gamma_i$  and centroid energy  $E_{ia}$ . Since the width of the resonance is usually very narrow compared to that of the electron beam energy, the profile function approximates a delta function. The cross section then becomes

$$\begin{aligned}\sigma_{aik}^{\text{DR}} &\sim \frac{\pi^2}{E_e} \frac{g_i}{2g_a} \frac{A_{ik}^r A_{ia}^a}{A_i^r + A_i^a} \delta(E_e - E_{ia}) \\ &= S_{aik} \delta(E_e - E_{ia}).\end{aligned}\quad (2)$$

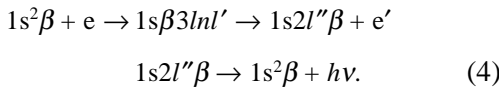
Here,  $S_{aik}$  is the resonance strength for the  $aik$  DR process which is given as the integral of the cross section over electron energies.

When the incident electron energy increases, the direct excitation (DE) transitions can occur to upper  $nl$  bound states. According to multiconfiguration Dirac-Fock (MCDHF) calculations for He-like Fe ions, the first excitation energies to  $1s2l$  and  $1s3l$  states are 6633.99 eV and 7860.63 eV, respectively. For the electron energies from 6.6 keV to 7.8 keV, X-ray signals are observed through the following processes,



Therefore, the X-ray spectra are analyzed by the calculations for the DE cross sections. In the calculation, the distorted-wave approximation (DWA) method was used and the potential was chosen to be the same as that for the bound state.

The energy region 6.6 keV – 7.8 keV also includes the process to form  $1s\beta 3lnl'$  ( $n \geq 3$ ) doubly-excited states. The decay process from  $1s\beta 3lnl'$  states is relatively complicated. Besides direct radiative decays to singly-excited states, which are too weak to observe, there are two other decay routes. One way is an autoionizing decay to form the excited state followed by radiative stabilization, shown as,

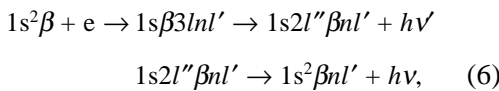


The upper process is called Resonance Excitation (RE), whose cross section can be calculated by

$$\sigma_{aik}^{\text{RE}} = \frac{\pi^2}{E_e} \frac{g_i}{2g_a} \frac{A_{ia}^a A_{ib}^a}{A_i^r + A_i^a} \delta(E_e - E_{ia}), \quad (5)$$

where  $b$  shows one of  $1s2l''\beta$  states.

Another way to achieve the  $2l'' \rightarrow 1s$  transition is the following successive radiative decays,



which is called Resonance Recombination (RER). Since  $1s2l''\beta nl'$  states are still doubly-excited states and can

decay through radiative or autoionizing transitions, an additional branching ratio should be multiplied in the calculation of RER cross sections as follows,

$$\begin{aligned}\sigma_{aik}^{\text{RER}} &= \frac{\pi^2}{E_e} \frac{g_i}{2g_a} \frac{A_{ia}^a}{A_i^r + A_i^a} \\ &\sum_{i'} \frac{A_{ii'}^r A_{i'k}^r}{A_{i'}^r + A_{i'}^a} \delta(E_e - E_{ia}),\end{aligned}\quad (7)$$

where  $i$  and  $i'$  are the states of  $1s\beta 3lnl'$  and  $1s2l''\beta nl'$  configurations, respectively. In the present calculations for RE and RER, the principal quantum number sum was truncated at  $n_{\text{max}} = 5$ .

Generally, incident electrons have an energy distribution and the cross sections should be convoluted using the energy distribution of the electron beam for comparison with experiment. In this paper, the electron beam energy distribution is approximated by means of a normalized Gaussian function:

$$f(E_e, E) = \frac{1}{\Delta\sqrt{\pi}} e^{-(E_e - E)^2 / \Delta^2}, \quad (8)$$

where  $\Delta = w/2\sqrt{\ln 2}$ ,  $w$  is the full-width-at-half-maximum (FWHM) of the electron beam energy distribution. The convoluted cross sections for various processes were calculated by means of the form:

$$\sigma^{\text{Conv}}(E_e) = \sum_q \frac{1}{\Delta\sqrt{\pi}} \int e^{-(E_e - E)^2 / \Delta^2} \sigma_q(E) dE. \quad (9)$$

In preceding discussions, all the photon-emission cross sections are given in  $4\pi$ -integrated form. In the EBIT, however, the electron beam is almost unidirectional, and the photon-emissions are detected at a direction perpendicular to the electron beam. The following relations are obtained for dipole transitions [5,14-17],

$$\begin{aligned}N(90^\circ) &= N_{\parallel} + N_{\perp} = \frac{3}{3-P} \langle N \rangle \\ \sigma(90^\circ) &= \sigma_{\parallel} + \sigma_{\perp} = \frac{3}{3-P} \frac{\sigma}{4\pi}.\end{aligned}\quad (10)$$

Here  $N(90^\circ)$  represents the photon numbers observed perpendicular to the beam,  $N_{\parallel}$  and  $N_{\perp}$  the number of photons polarized parallel and perpendicular to the beam, respectively.  $\langle N \rangle$  and  $\sigma$  are the  $4\pi$ -averaged photon numbers and the  $4\pi$ -integrated cross sections, respectively, and  $P$  the polarization degree. We calculated the polarization degrees for the intermediate-coupling eigen-states taking into account the relativistic spin-orbit interaction.

### 3. Comparison with Experiments and Discussion

For the experiment, the FWHM of the beam energy distribution,  $2\Delta\sqrt{\ln 2}$ , is in the range 20 eV – 90 eV. This value is greater than the energy differences between levels in a doubly excited configuration so the contribution to the total cross sections from individual levels can no longer be distinguished. Figure 1 shows the convoluted cross sections with a FWHM of 57.68 eV ( $\Delta^2 = 1,200$ ) for various processes of He-like ions. As shown in the figure, the DR processes are specified by labels KLL, KLM, and so on. For example, KLM means that an incident electron is captured into the M shell (or L shell) while the K bound electron is simultaneously excited to the L shell (or M shell).

The emitted photon numbers are proportional to the convoluted cross sections

$$\begin{aligned} \langle N \rangle &= \langle I_0 \rangle \sigma^{\text{Conv}} \\ N(90^\circ) &= 4\pi I_0(90^\circ) \sigma^{\text{Conv}}(90^\circ), \end{aligned} \quad (11)$$

where  $\langle I_0 \rangle$  and  $\sigma^{\text{Conv}}$  correspond to the  $4\pi$ -averaged photon number densities per unit area and the  $4\pi$ -integrated cross sections, respectively.  $I_0(90^\circ)$  and  $\sigma^{\text{Conv}}(90^\circ)$  correspond to  $90^\circ$  observation photon number densities and cross sections, respectively. They have relations as described in Eq. (10). The polarization degree  $P$  in Eq. (10) is a number between  $-1$  to  $1$  for each specified state depending on the angular momentum quantum numbers. The factor  $4\pi$  is for the purpose of keeping  $\langle I_0 \rangle$  and  $I_0(90^\circ)$  comparable (these have units of  $a_0^{-2}$  in our calculation).  $I_0(90^\circ)$  will be

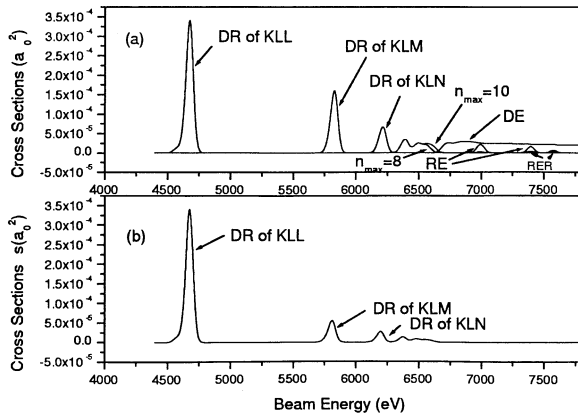


Fig. 1 a: Convoluted cross sections for various processes of He-like ions resulting in emission of  $2p \rightarrow 1s$  radiation. b: Convoluted DR cross sections of He-like ions due to outer electron decay. (FWHM = 57.68 eV)

discussed in detail in the following subsection 3.2. In subsequent discussions, we will compare the two kinds of results, *i.e.*,  $4\pi$ -averaged and at  $90^\circ$ , with the experimental spectra.

#### 3.1 $4\pi$ -averaged X-ray spectra

When we compare the total convoluted cross sections of He-like ions with the experimental result, using a roughly estimated  $\Delta$  and  $\langle I_0 \rangle$ , there appear two obvious differences. One of the differences is near 6,600 eV which corresponds to the energy absorption of high Rydberg states that were not included in our calculation. The other is in the high-energy tail of the KLL DR peak which shows evidence of the existence of other charge states.

For doubly excited configurations  $1s2l\beta n'l'$ , as  $n$  increases, the energy differences between neighboring configurations become smaller and, actually, for the Gaussian distribution function with approximately  $\Delta^2 = 1,200$ , the contribution to DR from  $n \geq 6$  configurations can no longer be distinguished, as shown in Figure 1(a). A comparison of the results for  $n_{\text{max}} = 8$  and  $n_{\text{max}} = 10$  in the figure shows that the convoluted DR cross sections for high Rydberg states may form a plateau that can join with the DE cross sections smoothly. This can be proved as follows: For high Rydberg states, the radiation probabilities of inner shell electron decay for doubly excited configurations become constants and the outer electron decay can be ignored, while the Auger decay rates decrease with  $n$  as  $n^{-3}$ . Thus, the branching ratio tends to unity, and the convoluted cross sections is given by

$$\sigma^{\text{CDR}}(E_e) = \sum_i \frac{e^{-(E_e - E_{ia})^2/\Delta^2}}{\Delta\sqrt{\pi}} \frac{\pi^2}{E_{ia}} \frac{g_i}{2g_a} A_{ia}^a. \quad (12)$$

The high Rydberg states may be regarded as pseudo continuum states in the rather wide electron beam energy width, since their energy separation is too narrow to resolve. If bound-state radial wavefunctions are renormalized such that their norm becomes inversely proportional to their energy separation at large principal quantum number  $n$ , the renormalized wavefunctions for a given angular momentum quantum number  $l$  converge to a zero-energy energy-normalized regular Coulomb function in the limit  $n \rightarrow \infty$ . The renormalization constant is given by  $\sqrt{d\epsilon_{nl}/dn}$ , where  $\epsilon_{nl} \approx -(Z - N + 1)^2/(2n^{*2})$  for the high Rydberg electrons.  $N$  denotes a number of bound electrons, and  $n^* = n - \mu_l$  the effective principal quantum number. The quantum defect  $\mu_l$  depends weakly on  $n$  for the high Rydberg states.

Auger decay is the inverse process of dielectronic electron capture and has the same transition matrix elements. The matrix elements for the dielectronic electron capture, in which an incident electron denoted by  $E_{ia}l'j'$  is captured into a Rydberg state denoted by  $nlj$  forming a doubly-excited autoionizing state  $i$  denoted by  $|bnljJ\rangle$ , may be expressed as

$$g_i A_{ia}^a = 2\pi (2J+1) \sum_{l'j'} |\langle bnljJ | \frac{2}{r_{12}} | | a E_{ia} l'j' J \rangle|^2, \quad (13)$$

where  $a$  and  $b$  represent the initial ionic target state and the excited ionic target states, respectively, and  $E_{ia} = E_i - E_a$  the resonance energy.  $r_{12}$  is the inter-electronic distance between the incident electron and an active electron of the target ion.  $J$  is the total angular momentum quantum number for the ionic target + electron system. The partial DE cross section, in which an incident electron denoted by  $E_e l'j'$  is scattered into a continuum state denoted by  $E_e - E_{ba} l'j'$  exciting the ionic target state from  $a$  to  $b$ , is given by,

$$\sigma_{ljJ}^{\text{DE}}(E_e) = \frac{\pi^3}{E_e} \sum_{l'j'} \frac{(2J+1)}{g_a} |\langle a E_e l'j' J | \frac{2}{r_{12}} | | b E_e - E_{ba} l'j' J \rangle|^2, \quad (14)$$

where  $E_{ba} = E_b - E_a$  is the excitation threshold energy. Thus, we obtain

$$F(E_{ia}) = \frac{\pi^2}{E_{ia}} \frac{g_i}{2g_a} A_{ia}^a \left( \frac{d\mathcal{E}_{nl}}{dn} \right)_{n \rightarrow \infty}^{-1} \sigma_{ljJ}^{\text{DE}}(E_{ba}). \quad (15)$$

The convoluted DR cross sections for high Rydberg states of Eq. (12) can be written as,

$$\sigma^{\text{CDR}}(E_e) = \sum_{nlj} \frac{e^{-(E_e - E_{ia})^2 / \Delta^2}}{\Delta \sqrt{\pi}} F(E_{ia}) \left( \frac{d\mathcal{E}_{nl}}{dn} \right) \approx \sum_{ljJ} \int \frac{e^{-(E_e - E_{ia})^2 / \Delta^2}}{\Delta \sqrt{\pi}} F(E_{ia}) dE_{ia}. \quad (16)$$

The last equation is obtained using an approximate relation  $E_{ia} = E_{ba} + \mathcal{E}_{nl}$ .  $F(E_{ia})$  is a function that varies slowly with  $E_{ia}$  and coincides with the DE cross sections at the threshold. As mentioned before, in our calculations, the potential used in the DWA calculation of the wave function is the same as that used for the bound states. Thus, the convoluted cross sections should be connected smoothly with that of the DE at the threshold.

Besides He-like ions, the DR of Li-like and Be-like ions may also contribute to photon emission of  $2p \rightarrow 1s + h\nu$ . The DR energies for those ions should shift a little

to the higher side from those for the He-like ions. Hence, the obvious difference between the convoluted KLL DR cross sections of He-like ions and experimental results can be attributed to missing contributions from the DR of the Li-like and Be-like ions.

The calculated cross sections for He-like ions, Li-like ions, and Be-like ions are given in Figure 2. One can see in the figure that the DR cross sections of different charge states merge as the principal quantum number of the outer electrons increases. Thus the mixing of Li-like and Be-like ions may cause little difference to the profile of the convoluted DR cross sections for high Rydberg states.

For the KLL DR cross sections, we fitted the linear combination  $\langle I_0 \rangle (c_{\text{He}} \sigma_{\text{He}} + c_{\text{Li}} \sigma_{\text{Li}} + c_{\text{Be}} \sigma_{\text{Be}})$  to the experiment spectra by using the least-square method. A set of fitting parameters,  $c_{\text{He}}$ ,  $c_{\text{Li}}$ ,  $c_{\text{Be}}$  and  $\langle I_0 \rangle$ , was determined self-consistently under the condition of  $c_{\text{He}} + c_{\text{Li}} + c_{\text{Be}} = 1$ . The parameters from the calculation are  $c_{\text{He}} = 0.75$ ,  $c_{\text{Li}} = 0.17$ ,  $c_{\text{Be}} = 0.07$ , and  $\langle I_0 \rangle = 5.1 \times 10^6 (1/a_0^2)$ . The  $c$  coefficients give the relative abundances of the ions. In a rapid scan of the electron energy, the ionization balance is considered to be constant for all energies. The effect of ion mixing is only obvious for KLL states. For very high Rydberg states, the difference between the cross section of He-like ions and mixed ions should be  $c_{\text{Li}} \times (\sigma_{\text{He}} - \sigma_{\text{Li}}) + \sigma_{\text{Be}} \times (\sigma_{\text{He}} - \sigma_{\text{Be}}) \sim 0.01 \rightarrow 0.02 \sigma_{\text{He}}$ . This is much smaller than the experiment resolution. Furthermore, the statistical experimental errors increase for higher beam energy where the signals are smaller, thus we will not discuss the effect of ion mixing for the range  $E_e > 6.6$  keV.

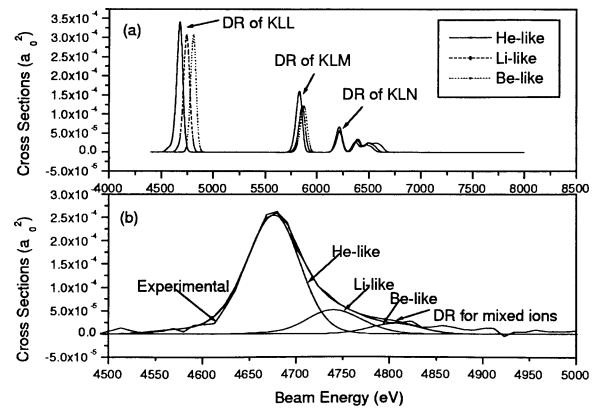


Fig. 2 (a): Convoluted inner shell decay DR cross sections for He-like, Li-like and Be-like ions. (b): Fitting with DR cross sections of He-like, Li-like and Be-like ions to the experiment for KLL states.

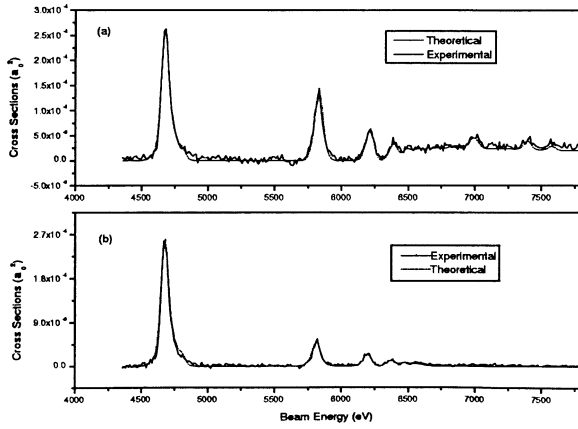


Fig. 3 (a): Total cross sections compared with experiment for the processes with  $2p \rightarrow 1s$  decay. The contribution from very high Rydberg states is obtained from interpolation. The DR cross sections are for mixed ions. The total cross sections above 6,634 eV are for He-like ions alone. (b): The comparison of convoluted DR cross sections of mixed ions with experiment for the processes with outer electron decay.

In Figure 3, the simulated photo-emission cross sections are compared with the experimental spectra. In the simulated cross sections, the mixing of Li-like and Be-like ions are taken into account using the mixing coefficients obtained from the least-square fitting of the KLL line profile. In the energy range above the first excitation threshold, the total cross sections of RE, RER, and DE processes were calculated for He-like ions alone. The DR cross sections for high Rydberg states  $1s2lnl'$ ,  $n = 11 \rightarrow \infty$  are obtained by interpolation. Close agreement is obtained for all energies in the figure.

Figure 4 shows the three-dimensional plot of the simulated X-ray spectra of  $4\pi$ -averaged as functions of beam energy and photon energy. The relative amplitude for all the transitions agrees approximately with the experiment as plotted in Figure 1 of Ref. [9].

### 3.2 $90^\circ$ observation and polarization effect

Since actually emitted photons were detected at  $90^\circ$  to the direction of the electron beam, for DR transitions of He-like, Li-like, and Be-like ions, we calculated the polarization degree for each radiative decay from doubly excited eigen states. The convoluted cross sections at  $90^\circ$  were obtained using Eq. (10) employing the calculated polarization degree. We fitted the expression  $I_0(90^\circ)(c_{\text{He}}\sigma_{\text{He}}^{\text{Conv}}(90^\circ) + c_{\text{Li}}\sigma_{\text{Li}}^{\text{Conv}}(90^\circ) + c_{\text{Be}}\sigma_{\text{Be}}^{\text{Conv}}(90^\circ))$  to the experimental spectrum. In the fitting procedure, all unknown parameters, *i.e.*,  $\Delta$ ,  $c$ 's and  $I_0(90^\circ)$ , were

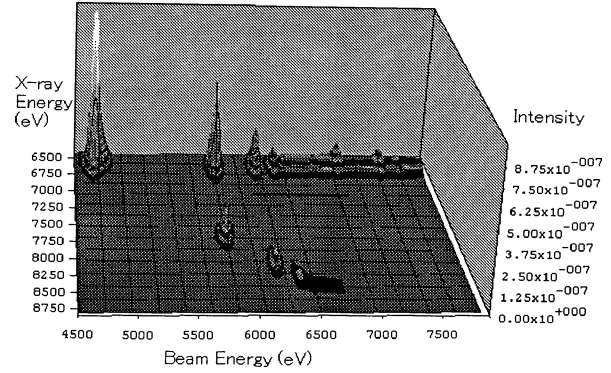


Fig. 4 A 3D-plot of the simulated spectrum using FWHM = 200 eV for photon energy.

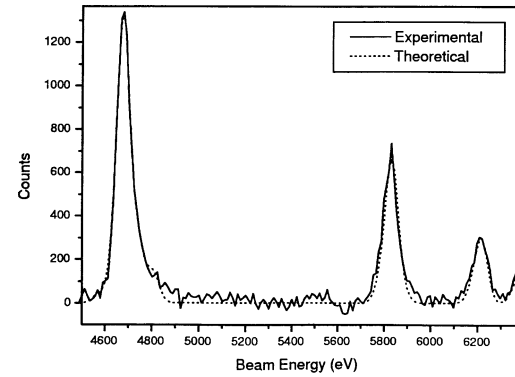


Fig. 5 Simulated DR spectra fitting to the experiment result for  $90^\circ$  observation.

determined simultaneously by using a non-linear least-square method [19] under the normalization condition:  $c_{\text{He}} + c_{\text{Li}} + c_{\text{Be}} = 1$ . Then we obtained  $\Delta^2$  of  $1188.9 \pm 60.9$  that corresponds to a FWHM of  $57.4 \pm 1.5$  eV for the electron beam energy,  $c_{\text{He}} = 0.740 \pm 0.001$ ,  $c_{\text{Li}} = 0.177 \pm 0.008$ , and then  $c_{\text{Be}} = 1 - c_{\text{He}} - c_{\text{Li}} = 0.082 \pm 0.009$  which were consistent with those for the space averaged cross sections. The result for  $I_0(90^\circ)$  was  $(4.45 \pm 0.06) \times 10^6(1/a_0^2)$ . The simulated spectrum with the obtained fitting parameters is given in Figure 5. Comparing Figure 5 with Figure 3, we find that the relative amplitudes of KLL, KLM, and KLN based on calculations are almost the same. The difference of  $I_0(90^\circ)$  and  $\langle I_0 \rangle$  from the fitting calculation is 13%. This means the average polarization degrees are very close for KLL, KLM, and KLN, which verifies the discussion in Ref. [9]. Since the ionized states may be regarded as the even higher Rydberg states that have the same angular quantum numbers for the dominant component in basis set expansion which determine the polarization degrees, the DE transitions may have approximately the

same average polarization degrees as KLM and KLN. Thus for the whole energy range, the average polarization degree is almost the same.

$N(90^\circ)$  of Eq. (11): the counts of photon-emissions detected at  $90^\circ$  in a solid angle  $d\Omega$  are proportional to the number of ions which have reacted in a volume  $V$ , multiplied by some detection efficiency  $p$ . Thus,

$$N(90^\circ) = pn_i n_e \bar{v}_e \tau V d\Omega \sigma^{\text{Conv}}(90^\circ), \quad (17)$$

where  $n_i$ ,  $n_e$ ,  $\bar{v}_e$  are ion and electron densities and an averaged electron velocity of the electron beam, respectively, which are virtually constant for an observation time  $\tau$ . The photon number density  $I_0(90^\circ)$  of Eq. (11) is written as,

$$I_0(90^\circ) = pn_i L \tau \frac{I_e}{e} \frac{d\Omega}{4\pi}, \quad (18)$$

where  $I_e$  is the electron beam current intensity, and  $L$  is the reaction length in the trap visible to the detector.

In the experiment, the electron beam current was 100 mA, the observable electron-ion interaction length was 1 cm, the observation time was 1.9 s for each electron energy channel, and the solid angle for the observation is approximately  $d\Omega = 4.01 \times 10^{-3}$ . Taking into account of the total efficiency of the detector system, which is estimated to be  $p = 0.5 - 0.6$  for  $h\nu \simeq 6$  keV based on the transparency [18] of the window in the front of the detector and the quantum efficiency of the detector (EURISYS MESURES EGP500-15), the

average ion density is estimated to be approximately  $6.5 - 8.5 \times 10^8 \text{ cm}^{-3}$ .

### 3.3 KLL spectra of high resolution

Each  $KLn$  ( $n = L, M, N, \dots$ ) resonance consists of several lines. In Table 1, calculated polarization degrees are listed for some KLL DR lines, and wavelengths and resonance strengths of those DR lines are compared [20-25]. As can be seen in the table, the polarization degrees depend on each transition. Thus, if we could observe the individual lines, strong polarization effects could be investigated in the spectrum. However, due to rather low spectral resolution, the measurement at the Tokyo-EBIT could not resolve each resonance into individual lines. It is inferred from the present calculations that the averaged polarization degree in each resonance is almost the same for all the  $KLn$  resonances. The relative amplitudes of the resonance peaks are therefore almost unchanged by taking into account the polarization effect. The individual KLL resonance lines were measured at  $90^\circ$  to the electron beam by Beiersdorfer *et al.* [5] using high-resolution X-ray spectroscopy. Using the calculated resonance strengths, polarization degrees, and ratio of reflection for different polarization direction listed in Ref. [18], we simulated the spectra. Figure 6 shows the simulation result and the measurements taken from [5].

In the calculation, both beam energy and photon energy distribution were regarded as Gaussian functions. However, since their actual energy resolutions were not

Table 1: Polarization degrees  $P$  and comparison of wavelengths  $\lambda$  (Å), photon energy  $h\nu$  (eV) and resonance strengths  $RS$  ( $10^{-20} \text{ cm}^2 \text{ eV}$ ) for He-like KLL DR radiation from Fe ions. Symbols are the same as those used in Ref. [5].

sym.	R decay	$P$	$(\lambda)_{a}$	$(\lambda)_{b}$	$(\lambda)_{c}$	$(\lambda)_{d}$	$RS_a$	$RS_e$	$RS_c$	$RS_f$	$RS_d$
o:	$1s2s^2 (^2S) ^2S_{1/2} \rightarrow 1s^2 2p \ 3/2$		1.8930	1.8946	1.8973	1.8963	0.850	0.91	0.82	0.94	0.84
		0.0	6549.77	6544.14	6534.82	6538.27					
p:	$1s2s^2 (^2S) ^2S_{1/2} \rightarrow 1s^2 2p \ 1/2$		1.8882	1.8894	1.8927	1.8918	0.829	0.92	0.80	0.91	0.85
		0.0	6566.42	6562.15	6550.7	6553.8					
e:	$1s2p^2 (^3P) ^4P_{5/2} \rightarrow 1s^2 2p \ 3/2$		1.8678	1.8724	1.8730	1.8721	4.04	4.28	4.12	4.32	4.80
		0.5	6637.89	6621.73	6619.6	6622.79					
j:	$1s2p^2 (^1D) ^2D_{5/2} \rightarrow 1s^2 2p \ 3/2$		1.8608	1.8594	1.8660	1.8654	27.04	29.15	27.22	26.27	26.90
		0.5	6662.97	6668.02	6644.43	6646.57					
r:	$1s2s2p (^1S) ^2P_{1/2} \rightarrow 1s^2 2s \ 1/2$		1.8590	1.8611	1.8640	1.8630	3.24	3.13	3.62	4.45	3.68
		0.0	6669.53	6661.93	6651.57	6655.14					
k:	$1s2p^2 (^1D) ^2D_{3/2} \rightarrow 1s^2 2p \ 1/2$		1.8583	1.8601	1.8631	1.8625	18.14	19.6	18.6	17.27	17.53
		0.6	6671.97	6665.51	6654.78	6656.92					
t:	$1s2s2p (^3S) ^2P_{1/2} \rightarrow 1s^2 2s \ 1/2$		1.8523	1.8535	1.8571	1.8565	5.50	6.35	5.83	5.28	5.77
		0.0	6693.69	6689.25	6676.28	6678.44					

a: This paper, b: Cornille [20], c: Chen [21], d: Vainshtein [22], e: Bely-Dubau [23], f: Nilsen [24]

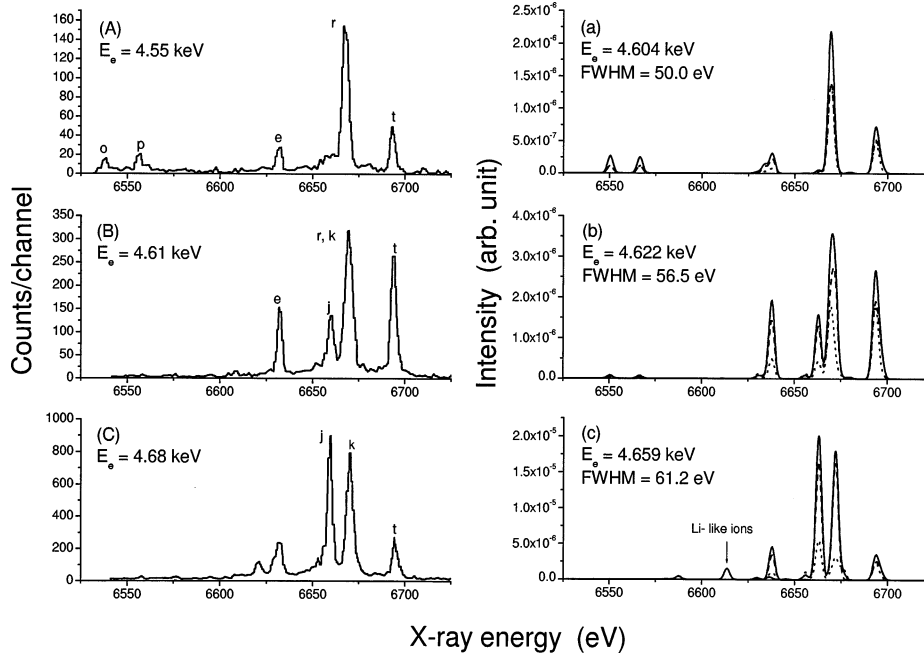


Fig. 6 (A), (B), (C): Experiment observation. (a), (b), (c): The simulated spectrum. Solid line, total intensity; dashed line, intensity associated with the parallel polarization; dotted line, intensity associated with the perpendicular polarization. A photon-energy resolution of  $\lambda/\Delta\lambda = 1,850$  is used for all the simulated spectra.

known, those values were treated as fitting parameters. There are also discrepancies for the position of spectra peaks. The main possible reason should be that, in the calculation of eigen energies of doubly excited states, configuration interactions with continuum states were not included. As well, strong interactions exist between bound configurations which means that the basis set states constructed from single electron wave functions are no longer accurate approximations. Thus the incompleteness of basis sets in the calculation may also increase the discrepancy. The X-ray energy differences from different calculations can be found in Table 1. Several hundred sets of parameters such as peak values and the widths of the electron beams, and the resolution of the photon detectors were before we found a close fit of each simulated spectrum to the measurement. From our calculation, the peak at an X-ray energy of 6637.5 eV in Figure 6(c) or (C) is due to the DR transition of He-like ions. The smaller peak at  $\sim 6620$  eV seen in the measurement could not be identified as any He-like line. It might be from Li-like ions, but the calculated energy value is 13 eV smaller than the corresponding experimental value. In Figure 6, the peak from Li-like ions was obtained by assuming that the density is the same as that of He-like ions.

The beam energies obtained by the fitting are

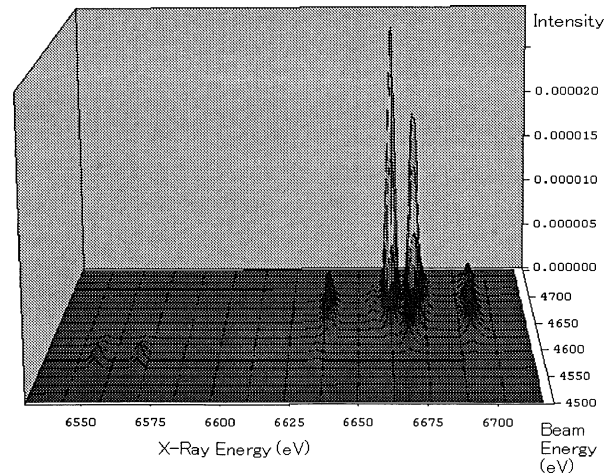


Fig. 7 Relative intensities of the KLL lines as functions of beam energy and photon energy.

different from those of the measurements. There might remain some uncertainty in the determination of the electron beam energy in the experiment. In this respect, it may be noteworthy that the relative intensities of the KLL lines have a potential importance for investigating the beam energy profile, *i.e.*, peak energy and energy width, since they depend strongly on the beam energy profile. Since in our simulation the FWHM of the beam

energy increases with the beam energy as can be seen in Figure 6(a), (b), and (c), we approximate  $\Delta^2$  by a parabolic function of the beam energy. The parameters of the parabolic function were determined based on simulation of (A), (B), and (C) in Figure 6. Together with the other parameters obtained from simulation and the reflection ratios of the two different polarizations plotted in Ref. [18] which were also approximated by parabolic functions of the beam energy, the dependence of the relative intensities of the KLL lines on the beam energy and the photon energy is shown in Figure 7.

#### 4. Summary

The X-ray spectra from highly charged Fe ions interacting with electrons were calculated in the electron beam energy range from 4.3 keV to 7.86 keV, and compared with the experimental observations using the Tokyo-EBIT. For all the important processes in this energy range, cross sections were calculated using the DWA method in the isolated resonance approximation. The spectral simulation was made by convoluting the calculated cross sections with the Gaussian distribution having the given energy spreads for the electron beam and the X-ray detector resolution. In the simulation, the abundance and the density of lower charged ions mixed with the main component of He-like ions was determined. The simulated X-ray spectra well reproduced the experimental observations.

For KLL DR lines, we compared the calculation results with the high resolution measurements by Beiersdorfer *et al.* [5], taking into account the polarization effect for each line. The agreement between the present simulation and the measurements was also quite close.

#### Acknowledgements

The authors are grateful to the members of the Tokyo EBIT group for their helpful discussion. One of the authors (Yueming Li) is supported by a scholarship from Mombu-Kagaku-sho in Japan. Fred Currell thanks The Royal Society, UK, for travel support facilitating this collaboration.

#### References

- [1] I.D. Williams, Rep. Prog. Phys. **62**, 1431 (1999).
- [2] P. Beiersdorfer *et al.*, Paper presented at ICPEAC XVII, Brisbane, July 1991 section 7.
- [3] R.E. Marrs, M.A. Levine, D.A. Knapp and J.R. Henderson, Phys. Rev. Lett. **60**, 1715 (1988).
- [4] C.M. Brown *et al.*, Phys. Rev. **A40**, 4089 (1989).
- [5] P. Beiersdorfer, T.W. Phillips, K.L. Wong, R.E. Marrs and D.A. Vogel, Phys. Rev. A **46** 3812 (1992).
- [6] F.J. Currell *et al.*, J. Phys. Soc. Japan **65**, 3186 (1996).
- [7] H. Watanabe *et al.*, J. Phys. Soc. Japan **66**, 3795 (1997).
- [8] H. Kuramoto *et al.*, Rev. Sci. Instrum. **71**, 687 (2000).
- [9] H. Watanabe, F.J. Currell, H. Kuramoto, Y.-M. Li, S. Ohtani and B. O'Rourke, J. Phys. B (Accepted).
- [10] R.D. Cowan, *Theory of Atomic Structure and Spectra* (University of California Press, Berkeley, CA, 1981).
- [11] Y.-M. Li and S. Li, J. Korean Phys. Soc. **32**, 312 (1998).
- [12] I.P. Grant, B.J. McKenzie, P.H. Norrington, D.F. Mayers and N.C. Pyper, Comput. Phys. Commun. **21**, 207 (1980).
- [13] H. Zhang, D.H. Sampson and A.K. Mohanty, Phys. Rev. A **40**, 616 (1989).
- [14] M.K. Inal and J. Dubau, J. Phys. **B22**, 3329 (1989).
- [15] A.S. Shlyaptseva, R.C. Mancini and P. Neill, Phys. Rev. A **57**, 888 (1998).
- [16] A.S. Shlyaptseva, R.C. Mancini and P. Beiersdorfer, J. Phys. B **32**, 1041 (1999).
- [17] A.S. Shlyaptseva, R.C. Mancini and P. Neill, Rev. Sci. Instrum. **68** (1), 1095 (1997).
- [18] B.L. Henke, E.M. Gullikson and J.C. Davis, At. Data Nucl. Data Tables **54**, 181 (1993).
- [19] W.H. Press, S.A. Teukolsky, W.T. Vetterling and B.P. Flannery, *Numerical Recipes in Fortran 77* (Cambridge University Press, NY, 1989) p. 675.
- [20] M. Cornille, J. Dubau, M. Loulergue, F. Bely-Dubau, P. Faucher, U.I. Safronova and A.S. Shlyaptseva, J. Phys. **B21**, 3347 (1988).
- [21] M.H. Chen, At. Data Nucl. Data Tables **34**, 301 (1986).
- [22] L.A. Vainshtein and U.I. Safronova, At. Data Nucl. Data Tables **25**, 49 (1978).
- [23] F. Bely-Dubau, J. Dubau, P. Faucher and A.H. Gabriel, Mon. Not. R. Astron. Soc. **198**, 239 (1982).
- [24] J. Nilsen, At. Data Nucl. Data Tables **38**, 339 (1988).
- [25] T. Kato, U.I. Safronova, A.S. Shlyaptseva, M. Cornille and J. Dubau, NIFS-DATA-24, 1995 (National Institute for Fusion Science).